Proceedings, 7th African Rift Geothermal Conference
Kigali, Rwanda 31st October – 2nd November 2018

Edge detection and 3-D Gravity Inversion at Kinigi Geothermal Field, Rwanda

Jean d'Amour UWIDUHAYE[1], Hakim SAIBI[2] and Hideki MIZUNAGA[3]

[1]Energy Development Corporation Limited, P.O. Box 3855 Kigali, Rwanda

[2]Geology Department, United Arab Emirates University, Al-Ain, United Arab Emirates

[3]Kyushu University, Japan

jduwiduhaye@edcl.reg.rw, damouru@gmail.com; mizunaga@mine.kyushu-u.ac.jp; hakim.saibi@uaeu.ac.ae

Keywords:

Gravity anomaly, CET analysis, 3-D Euler, 3-D inversion, Kinigi geothermal field.

ABSTRACT

This study investigates the geological structures, density distribution and crustal thickness of Kinigi geothermal area using gravity data. Gravity data set used in this study consists of 184 gravity stations surveyed in 2015 by West Japan Engineering Co. company and the first author. To achieve this, the Centre for Exploration Targeting (CET) Grid Analysis, Three-dimension (3-D) Euler, horizontal gradient and 3-D inversion methods were applied to gravity data. The complete Bouguer anomaly map was produced as it reveals density changes in the subsurface. Low gravity anomalies are observed in southwest of the area and high gravity anomalies in northeast and northwest of the area. The results from this study provide with new information that enhance the knowledge on the geological structures of the study area. Different lineaments were determined using the CET grid and derivative analysis, trending mainly in N-S and NNE-SSW. Based on the relationship between Bouguer gravity anomaly and crustal thickness, the Moho depths are ranging from 34.8 km to 36.06 km. The 2-D spectral analysis of gravity data shows two layers meaning deeper layer with depth of 1.8 km and shallower layer with depth of 0.5km. The interpreted map of lineaments is very useful for geological mapping, geothermal exploration and hydrogeological studies.

1. Introduction

Kinigi prospect is located in the Volcanic range, Northeast of Karisimbi volcano and between Bisoke and Sabyinyo volcanoes. Kinigi Geothermal field is one of three prospects located in North-Western of Rwanda (e.g. Brown, 2011; Shalev et al., 2012). The topography of study area is dominated by plateau, valleys, volcanis cones and volcanoes of 2 Km to 4 Km range in elevation (Jolie et al., 2009).

Different geo-reconnaissance studies (i.e geophysical, geological and geochemical) have been carried out in Kinigi to examine existance of geothermal resources (e.g; Chevron, 2006; Rutagarama, 2009; Jolie et al., 2009; Shalev et al., 2012). Magnetotelluric (MT) and Transient Electromagnetic (TEM) surveys were conducted to study the resistivity structures in Kinigi prospects (e.g Jolie et al., 2010; Shalev et al., 2012). Preliminary results from 1-D and 2-D modelling of resistivity method revealed a high resistive layer on the top (i.e layer of volcanic rocks) and a low to intermediate second layer probably caused by volcanic sediments from earlier eruption episodes in Kinigi geothermal field. The deep anomalous body at the SW of resistivity cross-section from SE of Karisimbi volcano to foothill of Sabyinyo volcano in Kinigi geothermal field might be an artifact of interpolation (Shalev et al., 2012).

Three-dimensional (3-D) modeling of MT data in the Kinigi geothermal field showed a shallow low resistivity (possibly a clay cap) and a deep low resistivity interpreted as the heat source of the geothermal system due to possible intrusions of conductive plume (Shalev et al., 2012).

The geochemical studies of cold springs found in study area showed that these springs discharge a high amount of carbon dioxide and the results from this discharge followed by formation of travertine found in the area (Brown, 2011). Additional to these, salinity analysis of cold springs in the area showed that they derived from young rocks (Jolie et al., 2009).

In this study, gravity method is used to delineate the geological structures beneath Kinigi Geothermal field. The polynomial fitting method was used to separate the shallow gravity sources (residual anomalies) from deep gravity sources (regional anomalies). Horizontal gradient, Centre for Exploration Targeting (CET) grid analysis methods were applied to delineate subsurface density structures. By this study, the subsurface structures are investigated.

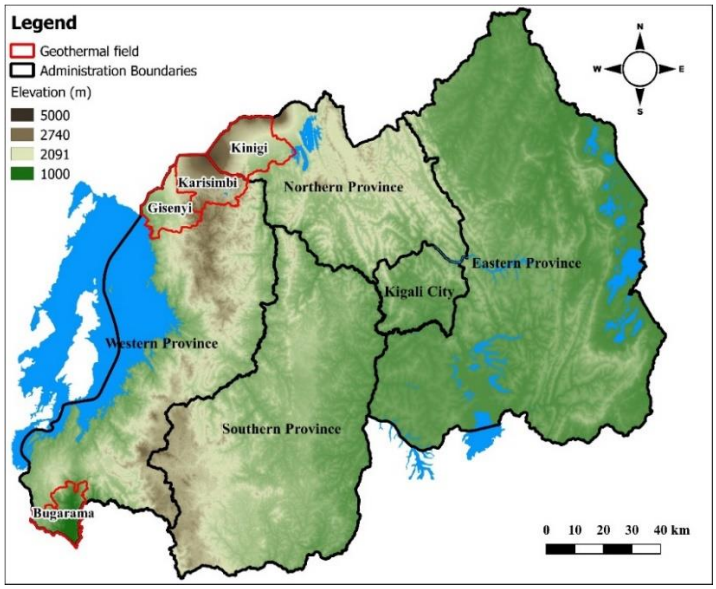

Figure 1: Location of Geothermal fields in Rwanda.

2. Geological Settings

Surface geology of Kinigi is dominated by fresh volcanic rocks erupted from Karisimbi, Bisoke and Sabyinyo volcanoes, these later are underlain by metasediments some of volcanic origin and possibly granitic intrusions (Shalev et al., 2012). Kinigi area is also contains thin lahars and debris flow from Sabyinyo volcano. In Rogers et al. (1998) petrography study, showed that the lavas present in Kinigi were characterized by the abundance of potassic alkaline rocks that consists of K-basanites, K-mugearites, leucitites, K-hawaiites and K-benmoreites. These young volcanic rocks overlie Mesoproterozoic basement complex comprising granites, pegmatites, gneisses and schists (Brown, 2011). Geological map is shown in Fig. 2.

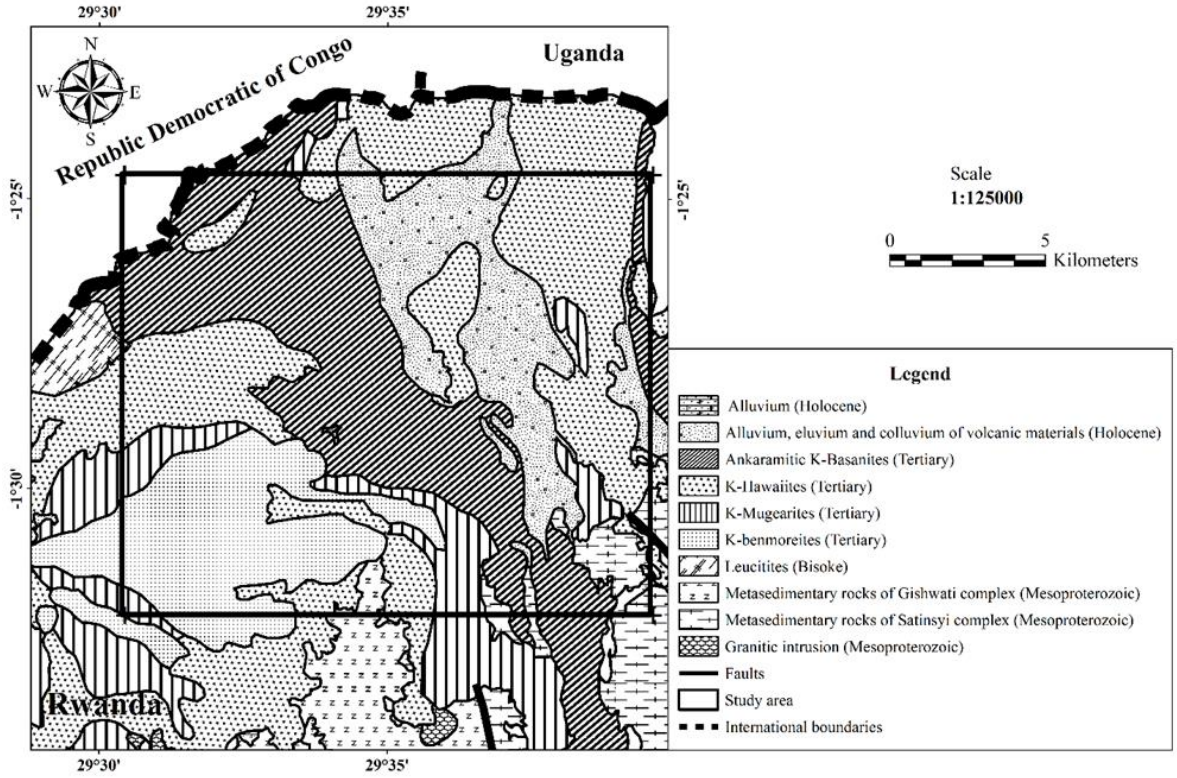

Figure 2: Geology map of the study area (modified after Theunissen et al., 1991).

3. Methodology

Gravity method is geophysical method used to study the earth's gravitational changes. The gravity method is a fast and effective geophysical tool for mapping subsurface structures. The minimum curvature method was used to grid the data. The Bouguer gravity anomaly map of the study area presents the general geologic features beneath Kinigi geothermal field (Fig. 3). Gravity lineaments from gravity anomaly map are used to interpret blind faults, contacts, and other tectonic and geological features. In this study, horizontal gradient, CET grid techniques were used to map density structures from gravity data. Additionally, 3-D Euler deconvolution and 2-D Power Spectrum methods were also applied to the gravity data to study the depth of fractures basement. 3-D inversion of gravity data was performed using GROWTH 2.0 software to retrieve a 3D model of the density contrast distribution from the study area.

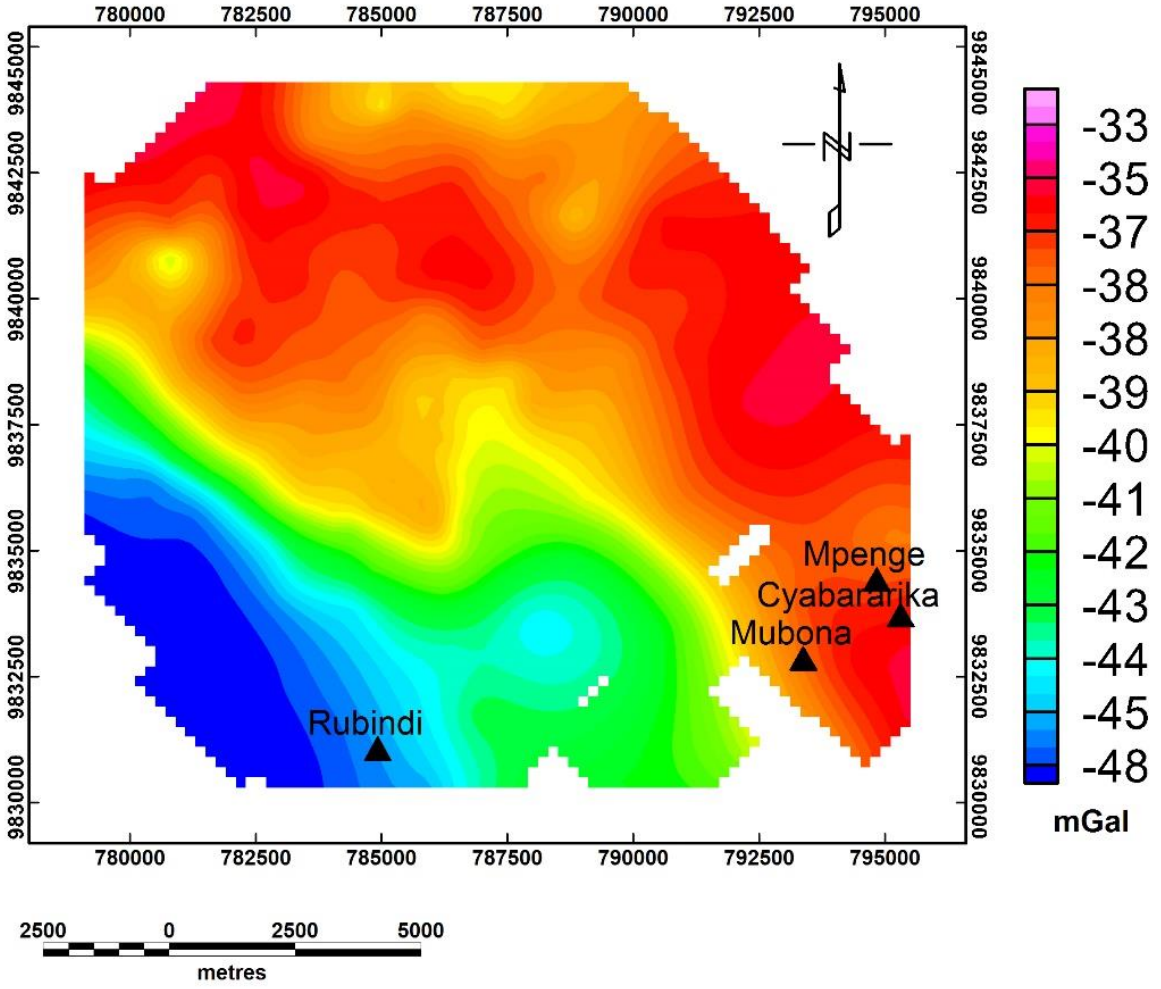

Figure 3: Complete Bouguer anomaly map in the study area. Triangles indicate springs in the area.

3.1 Horizontal Gradient method

Various authors presented and used horizontal gradient technique (HG) to locate density boundaries from gravity data (Blakely and Simpson, 1986; Ma et al. 2006). The horizontal gradient technique measures the variation of gravity field in a certain direction (e.g x or y). In 2-D, the horizontal gradient is calculated as follows:

$$\mathrm{HG} = \sqrt{\left(\frac{\partial g}{\partial x}\right)^2 + \left(\frac{\partial g}{\partial y}\right)^2} \quad (1)$$

Where $\partial g/\partial x$ and $\partial g/\partial y$ are the first horizontal derivatives of gravity field in *x*- and *y*-directions, respectively.

Horizontal gradient technique was used to generate horizontal gradient map in Kinigi area from residual anomalies of third trend. High anomalous zones of the horizontal gradient values are used to trace the trends of the gravity lineaments therefore

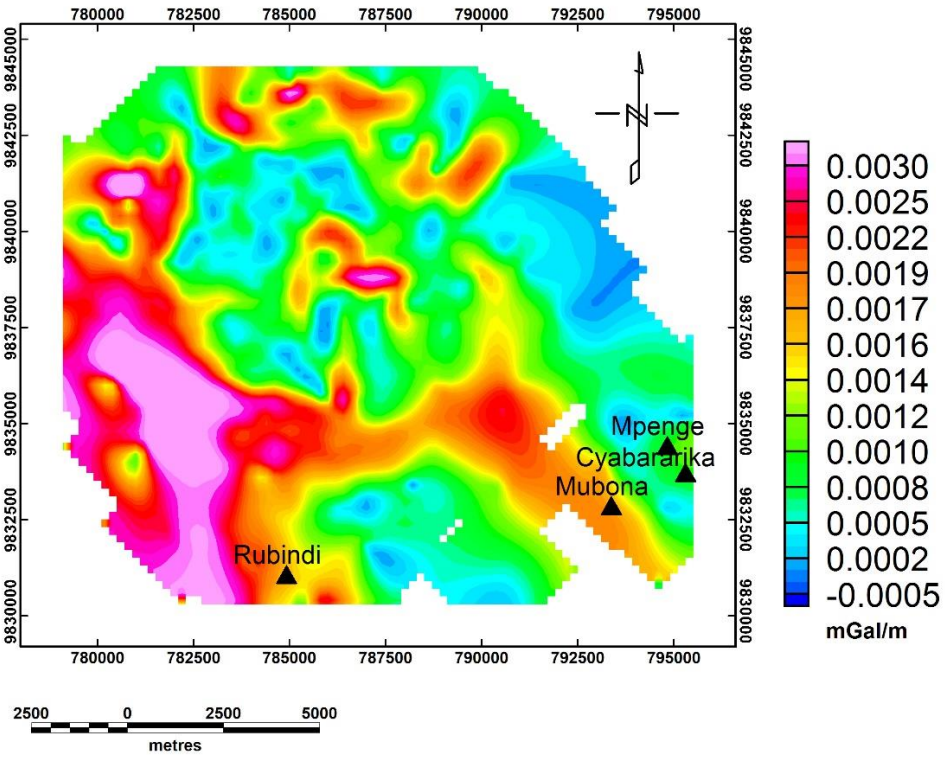

Figure 4: The horizontal gradient map of the residual anomaly of the Kinigi geothermal field.

3.2 Centre for Exploration Targeting Grid Analysis

CET grid analysis is a plugins tools for texture analysis, lineation detection, lineation vectorization, and structural complexity. It identifies the density discontinuity using combination of texture analysis and bilateral symmetric feature detection. These algorithms were developed by Holden et al. (2012). The Entropy plugin provides a measure of the textural information within localized windows (or neighborhoods) in a dataset. It measures the statistical randomness of a neighborhood data values by first quantizing the data into discrete bins and then analyzing the total number of distinct values resultant from that quantization.

Given a specified number of bins, *n*, for each cell *i* in a *k* x *k* sized neighborhood form a histogram and compute the entropy (*E*) as follows:

$$E = -\sum_{i=1}^{n} P_i \log P_i \tag{2}$$

Where the probability P_i is obtained after the normalizing the histogram of *n* bins. The output grid comprises real values indicating the amount of randomness exhibited by the texture in the neighborhood centred about each cell. Regions exhibiting high statistical randomness are considered high in entropy whereas regions of little randomness have low entropy.

The required parameters for such calculations include Window size and Histogram bins. In general, the window size for a grid with cell dimensions of 25 m x 25 m corresponds to an area of 125 m x 125 m. The number of histogram bins, denoted in the equation above as *n*. The default is 256 bins but this should be varied according to the range of data values in the grid.

For gravity datasets, it is suggested that a small milligal (mGal) range be allocated to each bin, e.g. 0.5 mGal. Note that the larger the number of bins, the greater the computation time.

CET phase symmetry algorithm are applied to the gravity data to enhance the appearance of linear features and therefore main trends/lineation can easily be mapped and traced.

In the texture-processed image, regions of gravity discontinuity are indicated by line-line features. One drawback with using standard edge detection methods to detect these features is that double responses are often returned for each line, as the methods are designed for locating step-edges rather than line features. Rather, contrast-invariant feature method was used to detect line-like features.

In this study, the phase symmetry edge detection was applied to the Bouguer anomaly of the study area (Fig. 3). Gravity data was converted to standard deviation grid from which window size of 5 x 5 was used to produce the phase symmetry map (Fig. 5).

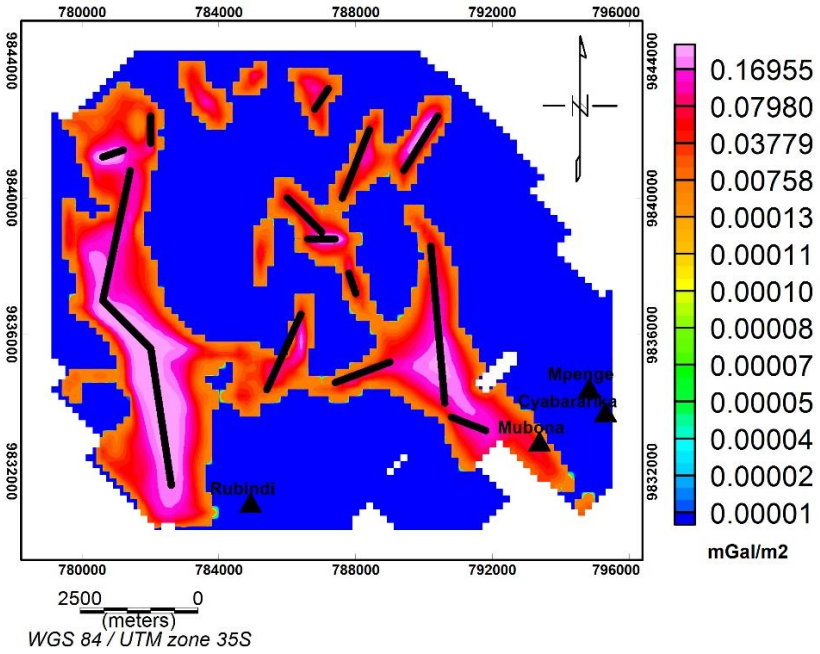

Figure 5: CET edge detection phase symmetry filter results deduced from gravity data.

3.3 3-D Euler Deconvolution

Euler deconvolution method has been discussed and used by various authors for depth estimation (e.g Thompson, 1982; Nabighian and Hansen, 2001; Mushayandebvu et al. 2004; Melo et al. 2013). The more details of the Euler deconvolution technique method and its application can be easily found in Reid et al. (1990), and Stavrev (1997). Euler depth solutions are used to estimate the source depth (z_0) and delineate the horizontal boundaries (e.g. Wilsher, 1987; Huang et al., 1995).

In 1982 Thomas discussed a new technique to estimates depths from real magnetic data along a profile. Euler deconvolution technique was used to estimate the source depth locations of the gravity or magnetic signature in a region; the 3-D Euler's differential homogeneity equation (Reid et al. 1990) is defined as follows:

$$(x-x_0)\frac{\partial g}{\partial x}+(y-y_0)\frac{\partial g}{\partial y}+(z-z_0)\frac{\partial g}{\partial z}=\eta(\beta-g) \tag{3}$$

which can be rewritten as:

$$x\frac{\partial g}{\partial x}+y\frac{\partial g}{\partial y}+z\frac{\partial g}{\partial z}+\eta g=x_0\frac{\partial g}{\partial x}+y_0\frac{\partial g}{\partial y}+z_0\frac{\partial g}{\partial z}+\eta\beta \tag{4}$$

where x_0, y_0, and z_0 are the source depth locations whose gravity field is measured at (x, y, z), β is regional value of the gravity and η is the Euler's structural index (SI), which defines the type of target used in the Euler deconvolution procedure, in other word it depends on the source geometry of the causative bodies. Structural index (SI) varies from 1 to 3 and require attention for the its selection based on the expected geological bodies and structure. Structural indexes can be used for many various geological situations (Reid et al. 1990).

In this study Euler deconvolution technique was applied to the gridded gravity data. Structural index (SI) used is 1 for sill edge, dike, or fault. The knowledge of the geology is very importance to accept Euler's solutions as Euler deconvolution generates many solutions. It has been observed that the source depth increases with increasing structural index.

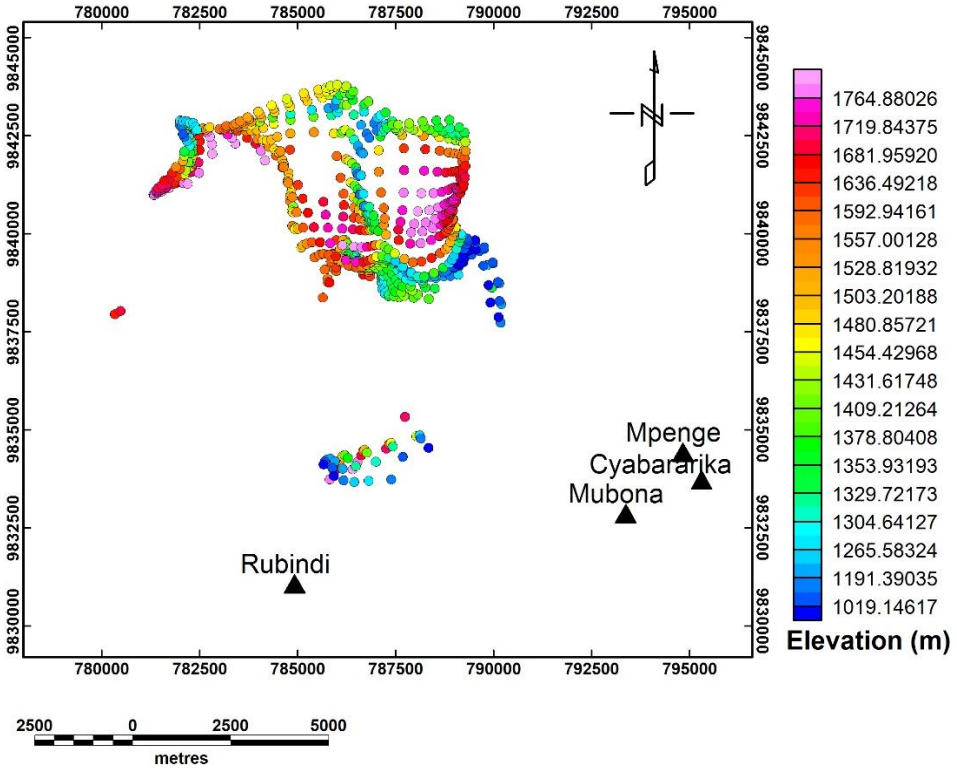

Figure 6: Standard Euler solutions (SI= 1) from gravity data.

3.4 Power Spectrum Analysis (PSA)

Before performing the 2-D Power Spectrum of gravity data, the Fast Fourier Transform (FFT) is applied to the gridded data to calculate a two-dimensional power spectrum curve (Fig. 7). Figure 7 shows the power spectrum of the gravity data.

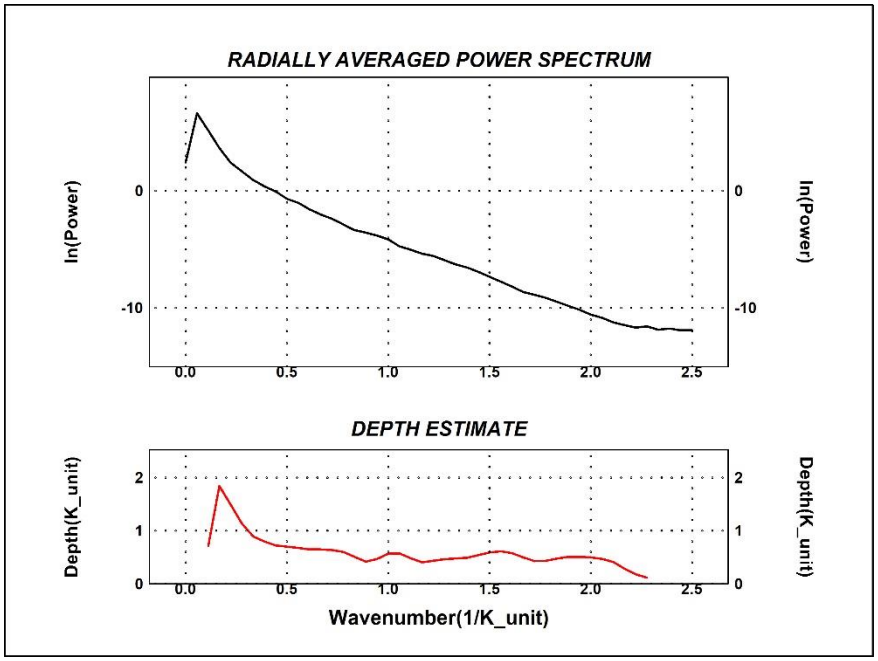

Figure 7: 2-D radially averaged power spectrum of the gravity data for the study area.

3.5 Moho depth estimation from gravity data

Moho depth can be estimated from gravity anomaly data. The empirical relationships between Bouguer anomaly and crustal thickness for whole earth was discussed and used by several authors (e.g Riad et al., 1981; Ram Babu, 1997, Rivero et al., 2002). Ram Babu (1997) presented the relationship as follows:

$$H=32-0.08\Delta g \quad (5)$$

where Δg is gravity anomaly, H is the Moho depth. In this study, the Moho depth was calculated using equation 5.

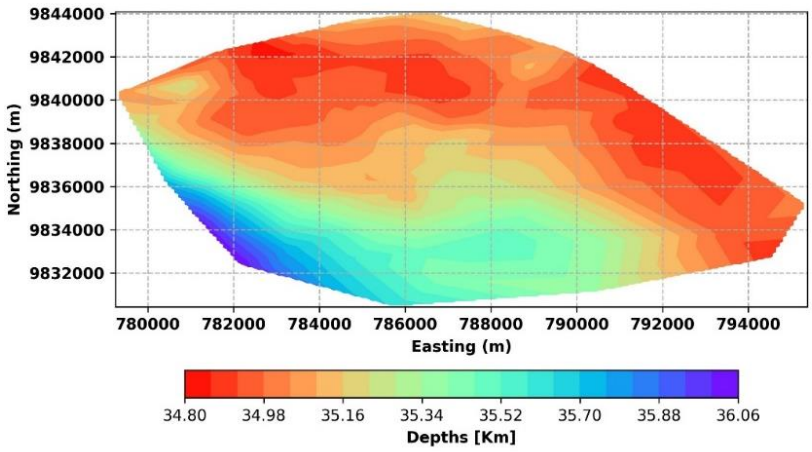

Figure 8: Moho depths in investigated area.

3.6 3-D Inversion

To study deeply anomaly at depth, 3-D inversion of gravity data was conducted as well as imaging the basement relief. The density structures of the subsurface in the study area have been defined using GROWTH 2.0 (Camacho et al. 2011).

We run the program GRID3D of GROWTH 2.0 and we accepted the default values such as: depth to the bottom of the model is -2652m and the length of the mean cell is 538 m. The GRID3D has detected 8423 cells. After that, we run the program GROWTH and accepted all default parameters such as: default density contrast (-400, +450 kg/m^3) and press the button "Adj" for free adjustment to a suitable value for the balance parameter. The program was executed and provided a model with a regional trend=-38.15 μGal. Finally, the model was accepted and we run VIEW program to develop the density contrast distribution beneath the study area and selecting different horizontals of the four main geothermal manifestations (Figure 9).

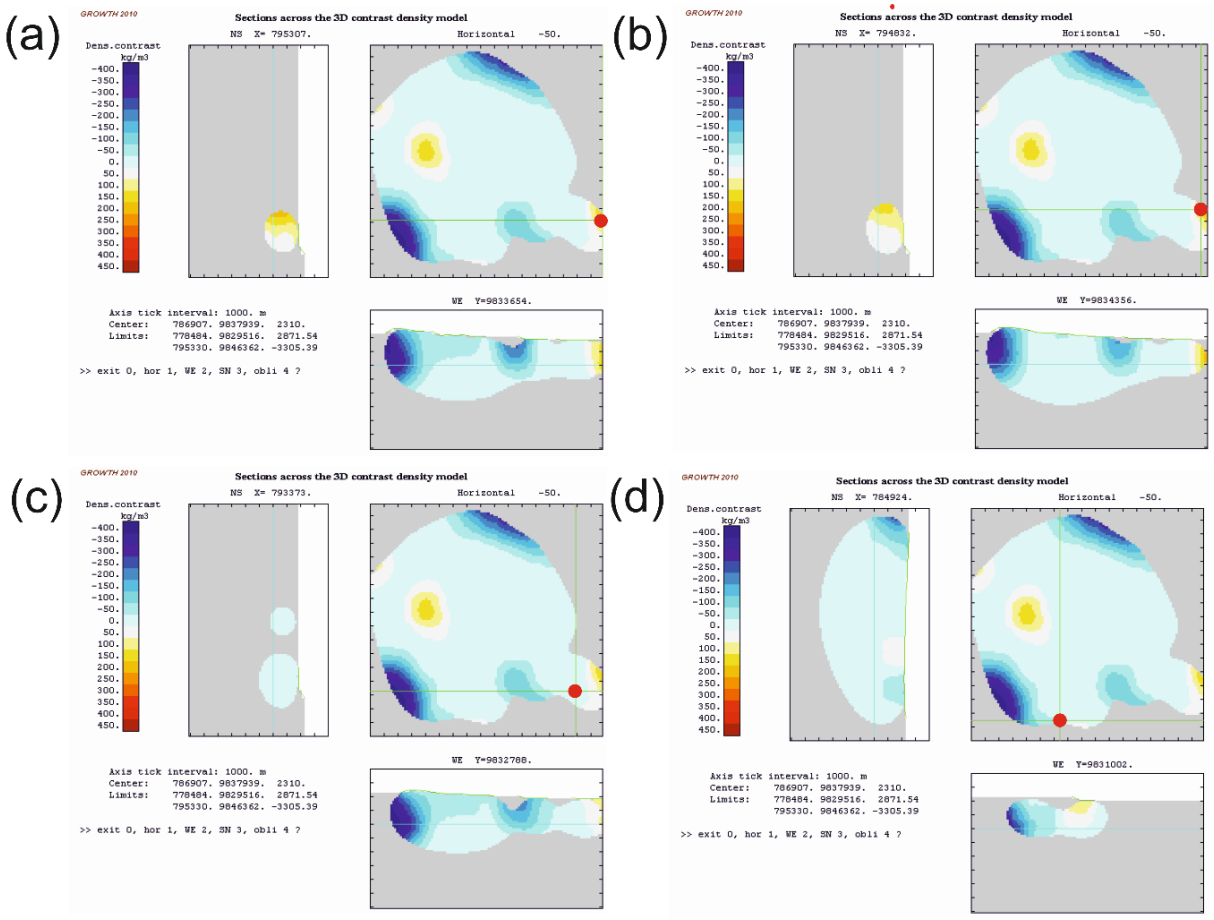

Figure 9: Horizontal and vertical cross-sections through subsurface density models in the study area at thermal springs. (a)= Cya spring, (b)=Mpenge spring, (c)=Mubona spring, (d)=Rubindi spring.

4. Results and Discussions

Bouguer anomalies of the area from -52 to -35 mGal (Fig. 3). Structurally, different gravity lineaments were estimated from horizontal and CET grid analysis methods in N-S, NNE-SSW and NW-SE directions. The HG map of the area (Fig. 4) showed gravity lineaments interpreted

as geological structures. The major trend is in N-S direction and high values are in SW part of the area. Notably, anomalies have elongated shapes which indicate various structural processes were occurred in the study area. The estimated structures are mainly oriented in NNE-SSW and in NNW-SSE directions. The edges of the main structures from CET Grid analysis are clearly shown at the maximum of the gradient value of gravity data (Fig. 5) and major trends are easily traced in N-S and NNE-SSW directions. The extracted lineaments from CET grid analysis were overlaid on the HG map (Fig.4) and as results, both have high level of agreement (Fig. 10) but the CET filter gave more clear results than the horizontal gradient. The changes in lengths of lineaments may be due to tectonic movement in the area.

The Euler source depth solutions shown in figure 6 range from 0.85 km to 1.93 km. In geological terms, the Euler depths represent the structural and/or stratigraphic changes of various geological formations i.e they appear wherever there are lithologic discontinuities. The results reveal two geological layers: 1) a deep geological layer with depth of 1.8 km and 2) shallow geological layer at about 0.5km depth.

The results from 3D Euler and power spectral of gravity data show good agreement. The two methods revealed two geological layers and depths: (1) shallower with 0.5 km to 0.85 km and (2) deeper with 1.8 km to 1.93 km depth.

The depth to the Moho boundary is ranging from 34.8 km to 36.06 km.

The crustal thickness map (Fig. 8) calculated from the gravity anomalies indicates that the crust in thicker in the SW of the area. These results are in reasonable agreement with the crustal map of Africa (Tedla et al., 2011).

The 3D inversion of gravity data showed that the thermal springs are located at boundaries of density changes ($\Delta\rho$ = +/- 50-100 kg/m^3) for Cya, Mpenge and Rubindi springs. Mubona spring is located at no density change area.

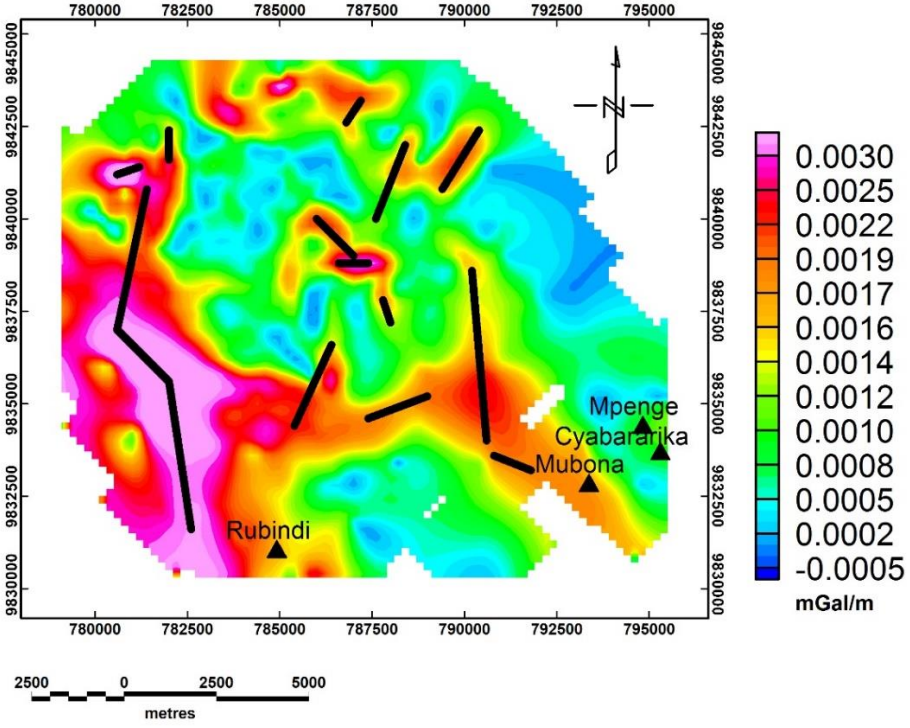

Figure 10: The integrated results of HG, CET.

5. Conclusions

The horizontal gradient, Centre for Exploration Targeting grid analysis methods were used in this study and the results revealed reliable gravity lineaments trending mainly in N-S and NNE-SSW directions and are interpreted as geological structure. The CET method proved to be clear than horizontal gradient method. The Moho depths of the area were estimated from the gravity data and the results are quite similar to the results presented by Tedla et al. (2011) with an average of 35.1 km. spectral analysis results showed two layers existing in the area. Table 1 shows the summary of results obtained in this study.

Method	**Results**
Horizontal Gradient (HG)	Geological structural trending in N-S, E-W and NE-SW
Centre for Exploration Targeting (CET)	Geological structural trending in N-S and NNE-SSW
Power Spectrum Analysis (PSA)	Shallow geological layer of 0.5 km depth Deep geological layer of 1.8 km depth
3D Euler Deconvolution	Depths to top of contacts ranging from 0.85 km to 1.93 km.
Moho Depths	34.8 0to 36.06 km
3D Inversion	Thermal springs are located at density contrast changes of +/- 50-100 kg/m^3

Table 1: Summary of results of this study.

REFERENCES

Blakely, R.J., and Simpson, R.W. "Locating edges of source bodies from magnetic or gravity anomalies. " *Geophysics*, 51, (1986), 1494-1498.

Browne, P. R. L. "Geothermal prospects in Rwanda. Institute of Earth Sciences and Engineering. " *IESE project report 1-2011.23618*, (May 2011).

Camacho, A.G., Fernandez, J., Gottsmann, J. "The 3-D gravity inversion package GROWTH2.0 and its application to Tenerife Island, Spain. " *Computers and Geosciences*, 37, (2011), 621-633.

Chevron. Preliminary assessment of Rwanda's Geothermal Energy Development Potential; report for Government of Rwanda. (2006)

Holden E.J., Wong J.C., Kovesi P., Wedge D., Dentith, M., Bagas, L. "Identifying regions of structural complexity in regional aeromagnetic data for gold exploration: An image analysis approach. " *Ore Geology Reviews*, 46, (2012), 47-59.

Huang, D., D. Gubbins, R.A. Clark, and K.A. Whaler (1995), Combined study of Euler's homogeneity equation for gravity and magnetic field. **In:** *57th EAGE Conference and Technical Exhibition; European Association of Exploration Geophysics*, Extended abstr., 144.

Jolie, E. "Geothermal Exploration in the Virunga Prospect, Northern Rwanda. " *Proceedings of the World Geothermal Congress*, Bali. (2010).

Jolie, E., Gloaguen, R., Wameyo, P., Ármannsson, H., A. Hernández Pérez, P. Geothermal Potential Assessment in the Virunga Geothermal Prospect, Northern Rwanda. Report Geotherm I, Federal Institute for Geoscience and Natural Resources (BGR). (2009)

Ma, Z.J., Gao X.L., Song Z.F. "Analysis and tectonic interpretation to the horizontal gradient map calculated from Bouguer gravity data in the China mainland." *Chinese Journal of Geophysics*, 49, (2006), 106-114.

Melo, F.F., Barbosa, V.C.F., Uieda, L., Oliveir, Jr., V.C., Silva, J. B. C. "Estimating the nature and the horizontal and vertical positions of 3D magnetic sources using Euler deconvolution. " *Geophysics* 78 (6), (2013), J87-J98.

Mushayandebvu, M.F., Lesur, V., Reid, A.B., Fairhead, J.D. "Grid Euler deconvolution with constraints for 2D structures. " *Geophysics* 69 (2), (2004), 489-496.

Nabighian, M.N., and Hansen, R.O. Unification of Euler and Werner deconvolution in three dimensions via the generalized Hilbert transform, *Geophysics*, 66 (6), (2001), 1805-1810

Ram Babu, H. V. "Average crustal density of the Indian lithosphere-an inference from gravity anomalies and deep seismic soundings. " *J. Geodyn*, 23 (1), (1997), 1-4.

Reid, A. B., Allsop, J. M., Granser, H., Millett, A. J., Somerton., I. W. "Magnetic interpretation in three dimensions using Euler deconvolution. " *Geophysics*, 55, (1990), 80-91.

Riad, S., Refai, E., Ghalib, M. "Bouguer anomalies and crustal structure in the Eastern Mediterranean. " *Tectonophysics*, 71, (1981), 253-266.

Rivero, L., Pinto, V., Casas, A. "Moho depth structure of the eastern part of the Pyrenean belt derived from gravity data. " *J. Geodyn*., 33 (3), (2002), 315-332.Rogers, N. W., James, D., Kelley, S., De Mulder, M. "The Generation of Potassic Lavas from the Eastern Virunga Province, Rwanda. " *Journal of Petrology*, 39 (6), (1998), 1223-1247.

Rutagarama, U. "Assessing Generating Capacity of Rwanda Geothermal Fields from Green Field Data Only. " *UNU-GTP*, Report 25, (2009).

Shalev, E., Browne, P., Wameyo, P., Palmer, J., Hochstein, M., Fenton R. "Geoscientific surveys of the Rwandan Kalisimbi, Gisenyi, and Kinigi Geothermal Prospects. " *Institute of Earth Science and Engineering (IESE) report for Rwanda*. (2012).

Stavrev, P.Y. "Euler deconvolution using differential similarity transformations of gravity and magnetic anomalies. " *Geophys. Prospect.* 45 (2), (1997), 207-246.

Tedla, G. E., Van der Meijde, M., Nyblade, A. A. and Van der Meer, F. D. "A crustal thickness map of Africa derived from a global gravity field model using Euler deconvolution. " *Geophys. J. Int.*, 187, **(**2011), 1-9.

Theunissen, K., Hanon, M., Fernandez-Alonso, M. "Carte Géologique du Rwanda (in French); Service Géologique, Ministère de l'Industrie et de l'Artisanat, République Rwandaise: Tervuren, Belgium, 1:250000. " (1991).

Thompson, D.T."EULDPH: A new technique for making computer-assisted depth estimates from magnetic data. " *Geophysics*, 47, (1982), 31-37.

Wilsher, W.A. "A structural interpretation of the Witwatersrand basin through the application of automated depth algorithms to both gravity and aeromagnetic data. " *M.Sc. Thesis, University of Witwatersrand, Johannesburg, South Africa*. (1987).